



Nanoscratch on mechanical properties of interfacial transition zones (ITZs) in fly ash-based geopolymers composites

Wengui Li^{a,*}, Zhiyu Luo^{a,**}, Yixiang Gan^b, Kejin Wang^c, Surendra P. Shah^d

^a School of Civil and Environmental Engineering, University of Technology Sydney, NSW, 2007, Australia

^b School of Civil Engineering, The University of Sydney, NSW, 2006, Australia

^c Department of Civil, Construction and Environmental Engineering, Iowa State University, IA, 50011, USA

^d Center for Advanced Construction Materials, The University of Texas at Arlington, TX, 76019, USA



ARTICLE INFO

Keywords:

Geopolymer
Interfacial transition zone (ITZ)
Nanoscratch
Deconvolution analysis
Friction coefficient

ABSTRACT

Interfacial transition zones (ITZs) of cementitious concrete are highly heterogeneous, which cause many challenges in accurately obtaining their properties. In this paper, regular aggregates were applied to prepare modelled geopolymers composites, in which ITZs exhibited neat boundaries. Nanoscratch technique with the ability to quickly scan a long distance was adopted to investigate mechanical properties of ITZ and geopolymers paste. To compare the properties of the ITZs and paste, abundant scratch data were analyzed in the form of histograms and Gaussian mixture models. The results showed that the ITZs in geopolymers with silica modulus of 1.5 presented similar properties with the paste, while the ITZs in geopolymers with silica modulus of 1.0 showed significantly higher scratch hardness but lower scratch friction coefficient than paste. Deconvolution analysis revealed that the abnormal hardness and friction coefficient of the paste in geopolymers with silica modulus of 1.0 could be caused by the defects related points. Compared with the traditional scratch scheme, the parallel scratch scheme based on modelled ITZ gave more stable results with a given number of test data, which can provide in-depth information for comparative studies.

1. Introduction

In recent years, the urgent need to develop green and low carbon construction materials has greatly promoted the research for alkali-activated fly ash geopolymers. Although there are numerous and various studies [1,2], the study on the interface transition zone between aggregate and paste of geopolymers is still limited. Among those limited studies, some favourable properties were found for ITZ in geopolymers. Lee [3,4] found that the ITZ between fly ash-based geopolymers paste and siliceous aggregates is not apparent when a high soluble silicate dosage was applied, and the system was salt-free. Comparative studies [5–7] also indicated that fly ash-based geopolymers concrete displayed better ITZ properties than Portland cement concrete. Different from Portland cement concrete, geopolymers concrete does not show significant debond between paste and aggregate and has both dense old and new interphase when using recycled aggregate [5,6].

One of the most important aspects to understand ITZ is its mechanical properties. Owing to the small width of ITZ, micro- and

nanomechanical test techniques [8,9] are important tools to quantitatively evaluate the properties of ITZs. Nanoindentation is the most widely used technique for this purpose and is generally performed in the form of grid nanoindentation [10–15]. Grid nanoindentation tests in the above comparative studies [5,6] revealed that for geopolymers concrete made with natural aggregate [5], the modulus and hardness of its ITZ were more heterogeneous than that in Portland cement concrete. When recycled aggregate was used, one study indicated that the ITZ between new paste and old mortar coated recycled aggregate in Portland cement concrete was about 20 μm according to the micromechanical distribution, but no obvious weak ITZs were found in geopolymers concrete [6], whereas another study found no distinct new ITZ in both Portland cement concrete and geopolymers concrete [16].

At present, the micro- and nanomechanical studies of ITZ in geopolymers are far from sufficient to reveal the complex properties of the geopolymers paste-aggregate ITZ. More quantitative mechanical properties results should be provided for a further understanding of the ITZs under different circumstances. For instance, when Na₂SiO₃ is not used,

* Corresponding author. School of Civil and Environmental Engineering, University of Technology Sydney, NSW, 2007, Australia.

** Corresponding author.

E-mail addresses: wengui.li@uts.edu.au (W. Li), zhiyu.luo-1@student.uts.edu.au (Z. Luo).

Table 1

Chemical composition of fly ash.

Oxide	Al ₂ O ₃	CaO	SiO ₂	Fe ₂ O ₃	K ₂ O	MgO	Na ₂ O	MnO	P ₂ O ₅	TiO ₂	LOI
Weight (%)	25.21	1.73	64.55	2.85	1.47	0.41	0.48	0.07	0.19	0.91	1.54

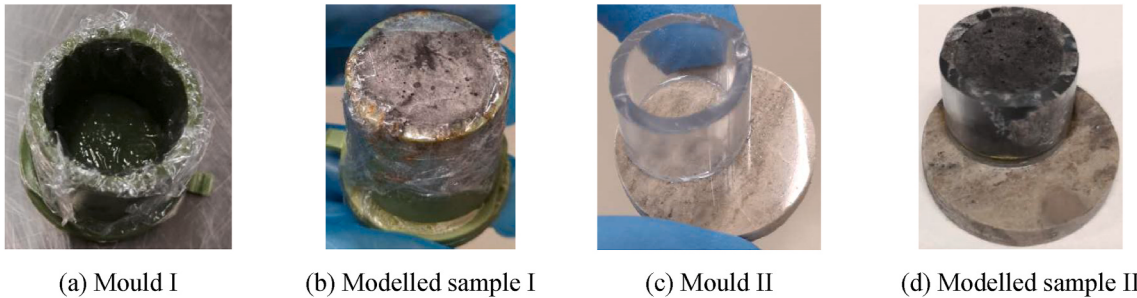


Fig. 1. Preparation of modelled samples for nanoscratch tests.

the microhardness of ITZ in alkali-activated slag concrete was even found lower than that in Portland cement concrete [17]. Similar studies should also be conducted for ITZs in fly ash-based geopolymers concrete to figure out the effects of crucial mix design parameters on the micro-mechanical properties of ITZs. The existing studies for ITZ in geopolymers are almost all based on indentation tests, which can only obtain limited test points due to the slow test speed. Besides, the ITZ studied is generally randomly chosen from an aggregate particle in concrete. Unlike the large scale tests that provide properties of bulk materials, the micro and nanoscale tests would be sensitive to the microscale heterogeneity of the tested materials and sometimes obtain just local properties. Thus, massive test points are necessary to adequately reflect the properties of the tested ITZ. Two types of modelled interface with a simplified interfacial condition were prepared in this study for the ITZ research. It could avoid the uncertainty caused by the “random choice” of ITZ samples in highly heterogeneous concrete for comparison study. Besides, it provides a neat ITZ. Scratch test with the ability to quickly measure material properties along a long line segment is introduced. Scratch test [8,18–22] has been used to investigate adhesion strength [23,24], abrasion resistant [25–28], fracture toughness [29–32], hardness [29,32,33], etc. Several studies used nanoscratch technique to study ITZ in Portland cement-based materials [8], which were mainly to measure the width of small scale ITZ between unhydrated cement grain and C-S-H [34,35]. In traditional research, scratch tests were performed across solid (e.g. cement grain), ITZ and paste. The scratch tests in this study were parallel to the neat boundary of the polished aggregate, which collected abundant test data from ITZ for comparison. The ITZ properties of the alkali-silica activated fly ash geopolymers with different silica modulus of 1 and 1.5 were investigated.

2. Experimental program

2.1. Raw materials and sample preparation

Geopolymer was synthesized by alkali-activation of low calcium fly ash. The chemical composition of Class F fly ash is listed in Table 1. Alkali solution adopted was the mixture of sodium hydroxide solution and sodium silicate solution. Sodium hydroxide pellets were dissolved into water and cooled down. Thereafter, it was incorporated into commercial D grade sodium silicate (14.7% of Na₂O, 29.4% of SiO₂ and 55.9% of H₂O) to adjust the silica modulus (SiO₂/Na₂O) from the original value of 2 to the widely used values of 1 and 1.5. For geopolymers samples with different silica modulus, they have the same Na₂O/fly ash of 8%, water/solid ratio of 0.33. A sand/fly ash ratio of 2 was used to prepare mortar samples. The geopolymers samples with different silica

modulus of 1 and 1.5 were denoted by the abbreviations of Geo-Ms1 and Geo-Ms1.5, respectively.

Coarse aggregate used was drilled from a limestone rock with calcite as the main component. The drilled φ25 mm long cylinder was cut into slices. The top and bottom sides of the slices were ground to parallel. These φ25 mm aggregate slices were further ground by abrasive papers to around 15 × 10 × 8 mm³ cuboids. The top side of the cuboid aggregate slices was polished to smooth by using 1 μm alumina for 20 min and put in a φ25 mm mould as shown in Fig. 1(a). For this type of mould, a layer of cling was stuck to it by using oil, which was designed to avoid the contact between geopolymers and mould, minimizing the damage of ITZ in the demoulding process. Afterwards, fresh geopolymers mortar was poured into the mould containing polished aggregate. The second type of modelled interface for ITZ observation was referenced from previous ITZ studies of Portland cement concrete [36]. As displayed in Fig. 1(c), one side of a φ10 mm vinyl tubing was polished to smooth and then glued to a polished surface of a φ25 mm aggregate slice to act as mould, which was poured with geopolymers paste. Both types of modelled samples were vibrated for 2 min and covered with cling. They were cured under 65 °C for 24 h in an oven and followed by standard curing until 28 days. The modelled samples obtained are provided in Fig. 1(b) and (d). After the demoulding, the modelled sample I was coated with epoxy resin and cut from top to bottom to expose a surface with neat ITZ. The surface was ground to flat by using 320, 600 and 1200 grits of abrasive paper and subjected to final polish with 1 μm alumina particles for 40 min and 0.3 μm alumina particles for 20 min. It was used for the nanoscratch test of ITZ. The modelled sample II was separated into two parts for the scanning electron microscope (SEM) observation of the interface between the surface of aggregate and residual geopolymers paste.

2.2. Characterization techniques

The width of ITZ in geopolymers samples was determined by grey-level threshold segmentation of backscattered electron (BSE) images [37]. The magnification of BSE images was determined as 500 × [38, 39]. For a segmented image, fourteen consecutive 5 μm strips cover ITZ and partial paste were taken starting at the boundary of aggregate. A total of forty such BSE images were adopted for statistics of the average proportion of components in strips. BSE was operated under an accelerating voltage of 15 kV by using Zeiss EVO LS15. SEM observation of ITZ in modelled sample II was conducted by Zeiss Supra 55VP with an accelerating voltage of 10 kV.

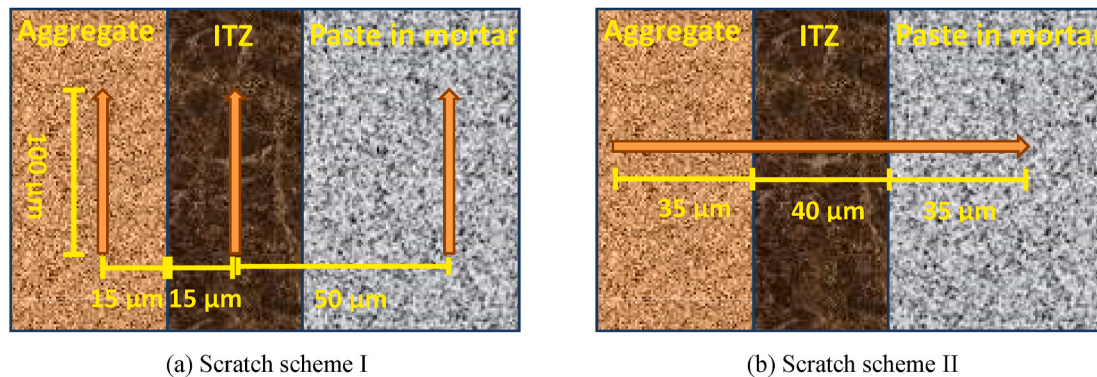


Fig. 2. Nanoscratch schemes for the ITZs.

2.3. Scratch technique

Scratch test was performed on Agilent G200 Nano Indenter by using a hemispherically-tipped, conical stylus. The radius and apex angle of this tip are 5 μm and 120°, respectively. It has the same apex angle but a far small radius compared with the representative tip (radius of 200 \pm 10 μm) in ASTM G171-03 (Standard Test Method for Scratch Hardness of Materials Using a Diamond Stylus) to facilitate the test on ITZ. For a real interface at the microscopic scale, due to the irregular shape of aggregate, the starting point of ITZ is likely to be a curved surface rather than a straight plane. In this study, as shown in Fig. 2(a), the neat aggregate boundary provided by modelled sample allows scratch to precisely test on “pure ITZ” to collect rich test data without incorporating properties results from aggregate and paste. According to the statistical results of BSE, the scratch tests on ITZ were set at 15 μm away from the boundary of aggregate. Tests were set on paste for comparison, which were 65 μm away from the boundary of aggregate. Regions with large cracks were avoided. For the first several ITZ tests, scratches with the same distance of 15 μm to the boundary were conducted on aggregate to help locate and observe scratch impression. The scratch paths were adjusted under a microscope to ensure that they were parallel to the aggregate boundary and started at the same level. The properties of ITZ and paste were both determined by twelve effective 100 μm scratches. In addition to the scratch test scheme I, parallel to the boundary of aggregate, as in Fig. 2(a) on individual objects, thirty three scratches based on the traditional scratch scheme II, perpendicular to the boundary, as given in Fig. 2(b) were conducted on geopolymers with a silica modulus of 1.5 to compare the test results.

To ensure the accuracy of the test, the normal load used should be moderately large. However, for the research here, an important factor limiting the normal load is the small width of the ITZ. The constraint effects of aggregate could possibly enhance the properties of ITZ.

significantly when the penetration depth is large. After a trial on a series of load levels, the final load for the scratch study of ITZ and paste was determined as 4 mN by referring to both ASTM G171-03 and the involved range of indentation test [40]. 2 mN and 8 mN scratch results on the more homogeneous modelled aggregate were also provided to help understand the effects of load levels. The tests on aggregate with different load levels were conducted at the location around 1500 μm away from the boundary of aggregate, which had the same scratch length and number as ITZ and paste tests. For all scratch tests, a constant scratch speed of 4 $\mu\text{m}/\text{s}$ was applied. Prescratch and postscratch scans were always performed at a small profiling load of 20 μN . The data acquisition rate is one point per micron.

According to ASTM G171-03, the scratch hardness HS_p based on this kind of tip can be determined by Eq. (1). Scratch friction coefficient μ was obtained by Eq. (2), based on scratch lateral force F_{scr} and normal force P . The geometric transition depth d_{gt} provided in Eq. (3) means a critical depth. When the test depth d is larger than this value, the test would involve the conical portion of the indenter tip. In this study, d_{gt} was calculated as 669.87 nm. For the test with depth-sensing technique, similar to a previous study [29], the scratch width w was obtained based on the geometry of the indenter and the depth acquired as given in Eq. (4). The scratch width w_{gt} under geometric transition depth was calculated as 5 μm , equal to the tip radius.

$$HS_p = \frac{8P}{\pi w^2} \quad (1)$$

$$\mu = \frac{F_{scr}}{p} \quad (2)$$

$$d_{gt} = r \left(1 - \sin\left(\frac{\alpha}{2}\right) \right) \quad (3)$$

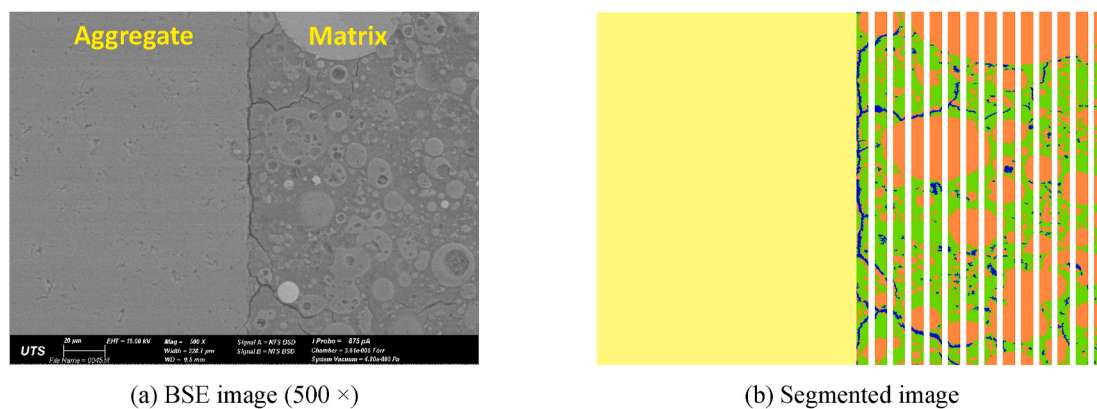
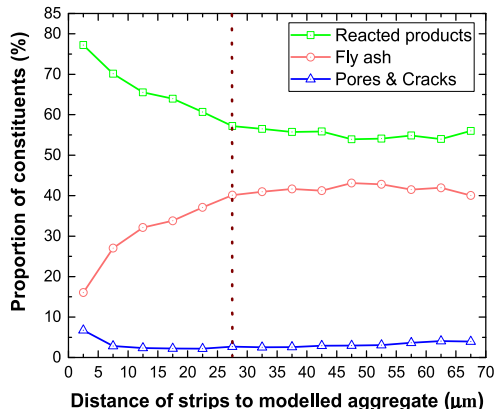
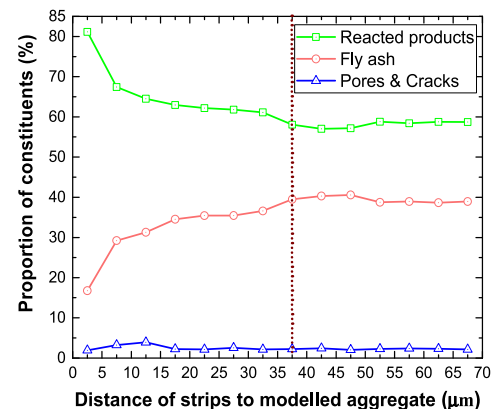


Fig. 3. Segmentation of BSE image based on grey value.

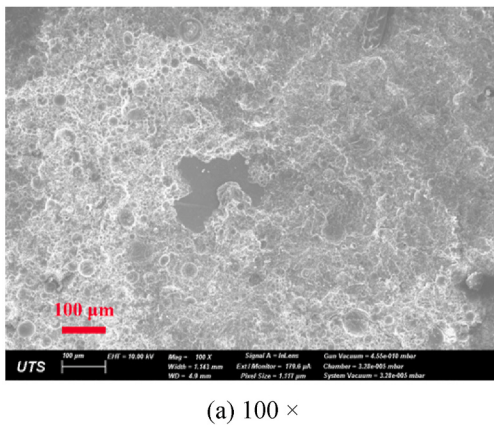


(a) Geo-Ms1

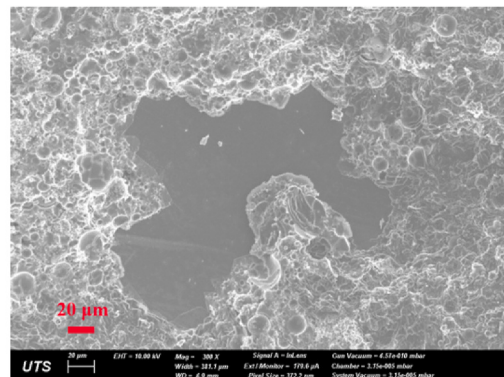


(b) Geo-Ms1.5

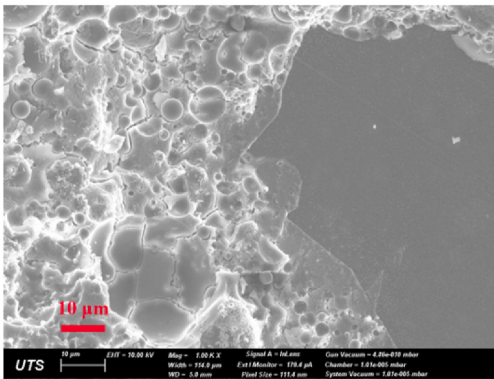
Fig. 4. Variation of constituents with increased distance to modelled aggregate (the dashed vertical lines indicate the boundary of ITZ and paste determined by BSE image analysis).



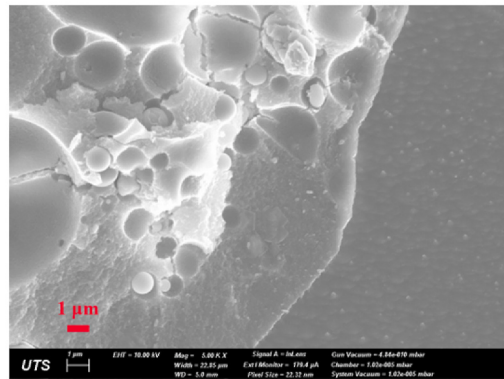
(a) 100 ×



(b) 300 ×



(c) 1000 ×



(d) 5000 ×

Fig. 5. Microstructures of ITZ in geopolymer with silica modulus of 1.5 on the aggregate surface.

$$w \begin{cases} \frac{2\sqrt{r^2 - (r-d)^2}}{w_{gt} + 2 \tan\left(\frac{\alpha}{2}\right)} \times (d - d_{gt}) & d \leq d_{gt} \\ d - d_{gt} & d > d_{gt} \end{cases} \quad (4)$$

where the value of α and r is 120° and $5 \mu\text{m}$, respectively, representing the apex angle of the conical portion and the radius of the hemispherical portion of the tip adopted.

3. Results and discussion

3.1. Determining ITZ by BSE

BSE images were segmented into three components of reacted products (green), fly ash (light red) and pores/cracks (blue) as revealed in Fig. 3. Pores on unreacted fly ash are sometimes unable to be precisely captured by grey values and incur inaccuracy when classified as pores manually. Therefore, they are still counted as fly ash in the part of BSE analysis. The ITZ in concrete is considered to be caused by the “wall” effect [36]. It means that the amount of unreacted fly ash would decrease whereas the solution to ash ratio would increase in ITZ due to

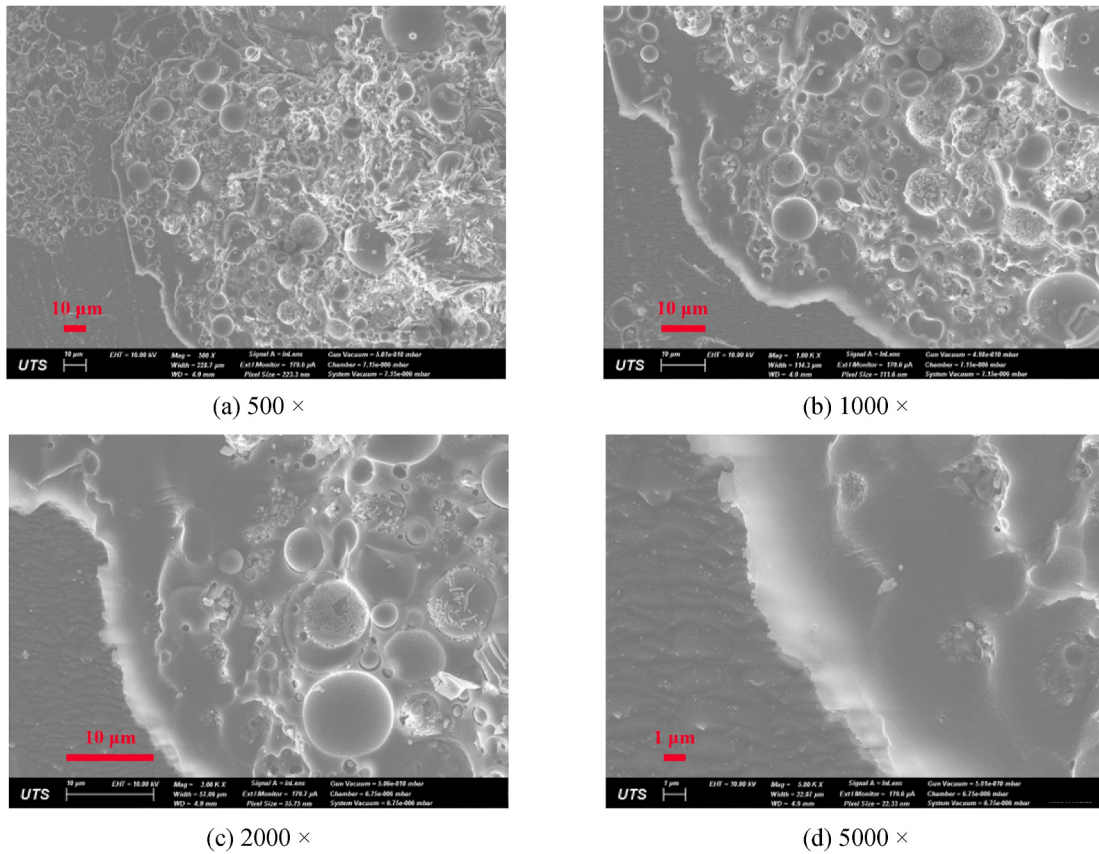


Fig. 6. Microstructures of ITZ in geopolymer with silica modulus of 1.0 on the aggregate surface.

the presence of aggregate as a wall. This phenomenon is clearly presented in the statistical results of BSE images as shown in Fig. 4, in which the proportion of constituents were plotted in the middle of the position of each strip. For geopolymer with different silica modulus, the distribution of constituents generally shows a similar trend. However, the “wall” effect is less significant in geopolymer with a higher silica modulus of 1.5. Besides, geopolymer with a silica modulus of 1 presents more unreacted fly ash and slightly more pores/cracks, but fewer reacted products than the sample with a higher silica modulus of 1.5.

For geopolymer with silica modulus of 1, the most significant part of ITZ was the first six strips, which corresponds to a width of around 30 μm . The increase of fly ash in geopolymer with silica modulus of 1.5 is less apparent. Nevertheless, it was identified that the increasing trend sustained until to 40 μm . Based on the results, the scratch test of ITZ was conducted at a distance of 15 μm to the boundary of aggregate.

3.2. Microstructure of ITZ

After separating bulk paste and aggregate of modelled sample II, abundant residual geopolymer paste was observed on the surface of aggregate as typically shown in Fig. 5(a) and (b) at low magnifications. The detail of the boundary was revealed in Fig. 5(c) and (d), where a dense and homogeneous binder can be observed at the region close to aggregate. Although the homogeneous features were magnified in Fig. 5 by the higher flowability of the solution than that of solids, it should still exist in actual ITZ because of the small liquid to solid ratio in ITZ. The change in silica modulus in this study did not bring significant differences for the observed results. For geopolymer with silica modulus of 1.0, a similar phenomenon is typically displayed in Fig. 6. The weak ITZ properties in Portland cement concrete is attributed to abundant pores and large crystals [36], which are related to hydration and high water to cement ratio in ITZ. For geopolymer, the usage of sodium silicate instead

of water has avoided these adverse factors. The high amount of residual geopolymer observed on aggregate actually indicates that geopolymer bonded tightly to aggregate. The interface would be sometimes stronger than the highly heterogeneous geopolymer bulk paste, which contains different types of smooth fly ash and microscale crystals [41,42]. For the modelled sample prepared, the bond between geopolymer and polished aggregate is weaker than that of geopolymer and field aggregate which has a rough surface. Thus, the same phenomenon of a good bond of geopolymer to aggregate could also occur in real geopolymer concrete.

3.3. Nanoscratch test results

3.3.1. Effects of load level

The 2 mN, 4 mN and 8 mN scratch loads were applied on the modelled aggregate. The obtained results for hardness and friction coefficient were presented in the form of frequency density histogram as displayed in Figs. 7 and 8. Although histogram varies with its bin size and it is difficult to find an appropriate bin size [41,42], the same bin size specified for all samples would be still feasible for the comparison purpose. In addition to histograms, the properties distribution was described as Gaussian mixture models, with the parameters determined by maximum likelihood estimation [41,42]. The number of components for models was increased until it can match the histogram well. Then, the models were used to represent the frequency density histograms and plotted in the same figure to facilitate comparison.

As revealed in Figs. 7(d) and Fig. 8(d), the results clearly indicate that both the hardness HSp and friction coefficient μ increased with load level P . The average value and standard deviation of test result data are given in Table 2. Friction coefficients are very small values in the range of 0.12–0.35, while hardness is around one order of magnitude greater than the friction coefficient, which varies between 1.95 GPa and 2.64 GPa. Although both hardness and friction coefficient increased with the

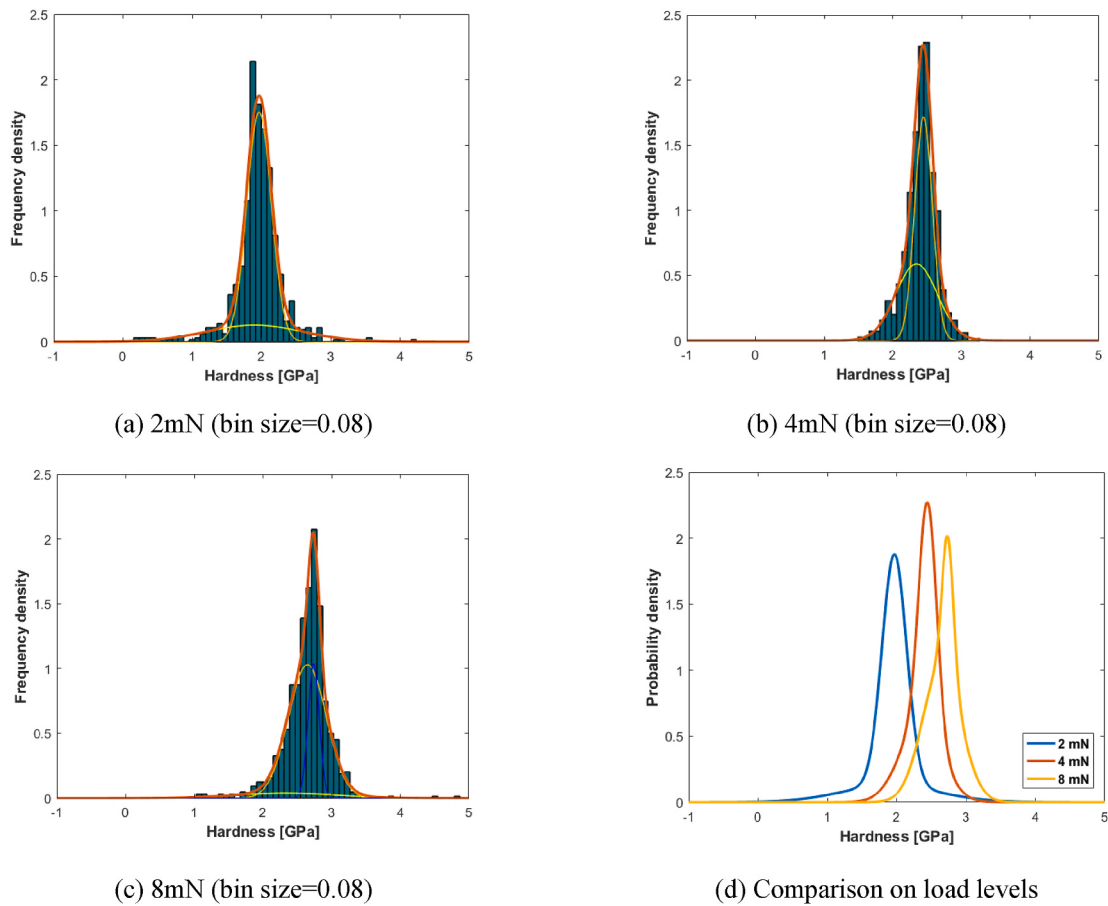


Fig. 7. Scratch hardness of aggregate at different load levels.

increase of normal load, their increasing trends are different. When the normal load was increased from 2 mN to 4 mN, the hardness and friction coefficient were increased by 23.08% and 41.67%, respectively. The corresponding increase from 4 mN to 8 mN is 10.00% and 105.88%, respectively. The load level is obviously more influential on the friction coefficient and causes less change in hardness. It could be attributed to the effects of surface defects under small load tests, which is especially significant for friction coefficient that governed by the topology of the contacted surface [29]. Since properties are dependent on test factors, the same scratch load and speed are set for the test of ITZ and paste.

3.3.2. Scratch hardness of ITZ and paste

Based on the constant load of 4 mN under test scheme I, the average value and standard deviation of hardness and friction coefficient results of ITZ and paste are obtained as listed in Table 3. ITZ and paste are found to have lower hardness but higher friction coefficient and standard deviation than that of aggregate when the same scratch load and speed were applied. The high standard deviation is caused by the distinct hardness of different constituents. For geopolymer with different silica modulus, results reveal that ITZ of Geo-Ms1.5 sample has almost the same hardness and friction coefficient as its paste, whereas the ITZ of Geo-Ms1 shows distinctly higher hardness but lower friction coefficient than paste. The hardness and friction coefficient of Geo-Ms1 are similar to or larger than that of Geo-Ms1.5. For heterogeneous samples, the comparative study cannot be just based on the average value. For instance, some types of fly ash have great mechanical properties but account for a small proportion. The scratch tests can not reflect the real proportion of the fly ash very accurately and hence affect the comparison results based on the average value. This aspect can be known by the largest hardness obtained by scratch, which is 52.49 GPa for Geo-Ms1-

ITZ, but just around 10 GPa or 35 GPa for other samples. Compared with unreacted fly ash, gel and defects are far more important constituents that would determine the macro performance of samples. Hence, deconvolution analysis was conducted for further discussion.

3.3.3. Properties comparison of ITZ and paste by deconvolution analysis

The scratch hardness of ITZ and paste in geopolymer samples with different silica modulus are displayed in Fig. 9. The deconvolution results for hardness are listed in Table 4. It can be observed that the Gaussian mixture models with 3 components match with corresponding frequency distribution histograms. Geopolymer is mainly composed of unreacted fly ash, N-A-S-H gel, crystals and defects (pores and cracks), where the proportion of the latter two is relatively small. Due to the large indenter tip adopted for scratch and the small characteristic size of some constituents, the deconvolution study is not expected to generate individual pure phases. However, the decomposition of Gaussian mixture models is still useful for the analysis of mechanisms. For the three components in each sample, the increased mechanical properties mean the increased test points from fly ash particles and crystals, and the decreased test points from gel and defects. The test points belong to the second and especially the third component should be mainly from fly ash particles. The test points in the first component with minimum hardness should be primarily from N-A-S-H gel. Compared with others, the first component is the least affected by fly ash/crystals and hence the key for comparative study. The results in Table 4 indicate that the first component of Geo-Ms1.5-ITZ and Geo-Ms1.5-paste has a similar value of around 0.94 GPa. However, the corresponding components in ITZ and paste of Geo-Ms1 present distinctly different hardness values, which are 1.10 GPa and 0.77 GPa, respectively. The discrepancy can also be clearly observed by the summarized distributions provided in Fig. 10.

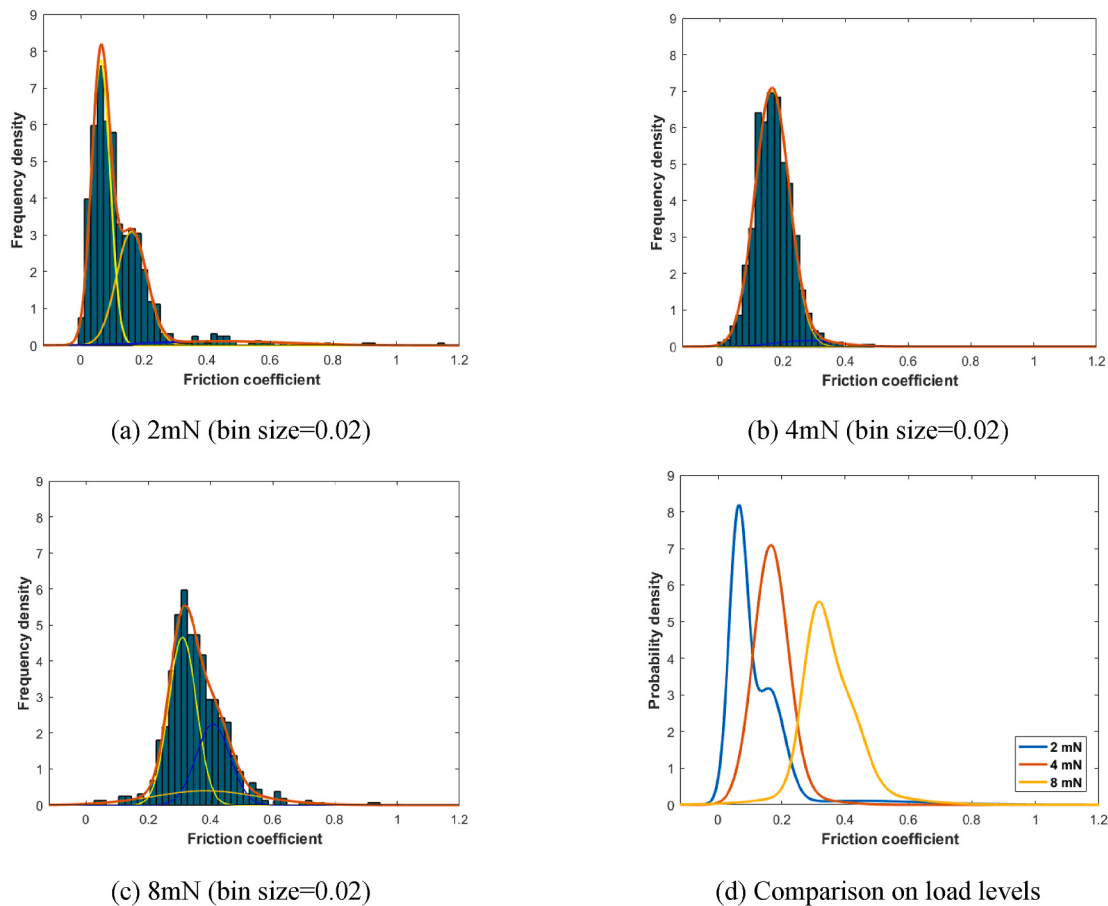


Fig. 8. Scratch friction coefficient of aggregate at different load levels.

Table 2

Average scratch hardness and friction coefficient of aggregate under different load levels.

Load level	Scratch hardness (GPa)	Scratch friction coefficient
2 mN	1.95 ± 0.37	0.12 ± 0.11
4 mN	2.40 ± 0.23	0.17 ± 0.06
8 mN	2.64 ± 0.33	0.35 ± 0.09

Table 3

Average hardness and friction coefficient of ITZ and paste with difference silica modulus.

Samples	Scratch hardness (GPa)	Scratch friction coefficient
Geo-Ms1.5-ITZ	1.38 ± 0.75	0.31 ± 0.30
Geo-Ms1.5-paste	1.39 ± 0.83	0.31 ± 0.27
Geo-Ms1-ITZ	1.72 ± 1.42	0.32 ± 0.29
Geo-Ms1-paste	1.49 ± 1.46	0.42 ± 0.37

In this study, 3 components were set for the convenience of comparison. To reveal more details, the number of components was increased for Geo-Ms1-paste. Further increasing the number of components was accompanied by a better match of probability density curve with frequency density histogram. When the number of components increased to 5, as shown in Fig. 11, the component with hardness of 0.77 was decomposed into two components with hardness of 0.58 GPa and 1.06 GPa, respectively. The deconvolution results for the 5 component model provided in Table 4 show that in addition to the small proportion, the second newly decomposed component with hardness of 1.06 GPa is

similar to the minimum component in other test objects. The lowest hardness of 0.77 GPa obtained in 3 component models for Geo-Ms1-paste should be caused by the first newly decomposed component with a small hardness of 0.58. This component should have a considerable amount of defects related test points (low strength gel). Defects such as some capillary pores in gel are not large enough to be detected by BSE analysis at the magnification of 500×, but would still affect scratch properties significantly.

Table 5 presents the percentage of test data from typical large scratch widths of larger than 5 μm ($H < 0.407$ GPa) and 4 μm ($H < 0.637$ GPa). Results in Table 5 indicate that the percentages are very close for Geo-Ms1.5-ITZ, Geo-Ms1.5-paste and Geo-Ms1-ITZ, which vary in the range of 1.66%–1.94% and 7.46%–8.65%, respectively. Larger proportions of 8.45% and 21.21% are found for Geo-Ms1-paste. For hardness data less than 0.407 GPa and 0.637 GPa in Geo-Ms1-paste, the proportions of data from the defects related phase ($H = 0.58$) can be estimated based on Eq. (5) and deconvolution results in Table 4, which were obtained as 89.56% and 84.27%, respectively. Thus, these results again indicate that the small hardness data in Geo-Ms1-paste are primarily from the defects related phase. It should be noticed that the defects related phase should still contain some normal gel points and the real differences in the proportion of defects between Geo-Ms1-paste and others may be less significant as manifested in Table 5. After all, the contact area of nanoscratch test at the small hardness point is very large, and the distance between adjacent test points is only 1 μm. Still, it can be pointed that the low strength gel caused by small defects are more in Geo-Ms1-paste.

Based on the scratch hardness results and SEM observation above, it can be found that the ITZ of geopolymers samples studied is not weaker than that of the paste. Besides, the silica modulus of 1.5 used makes the

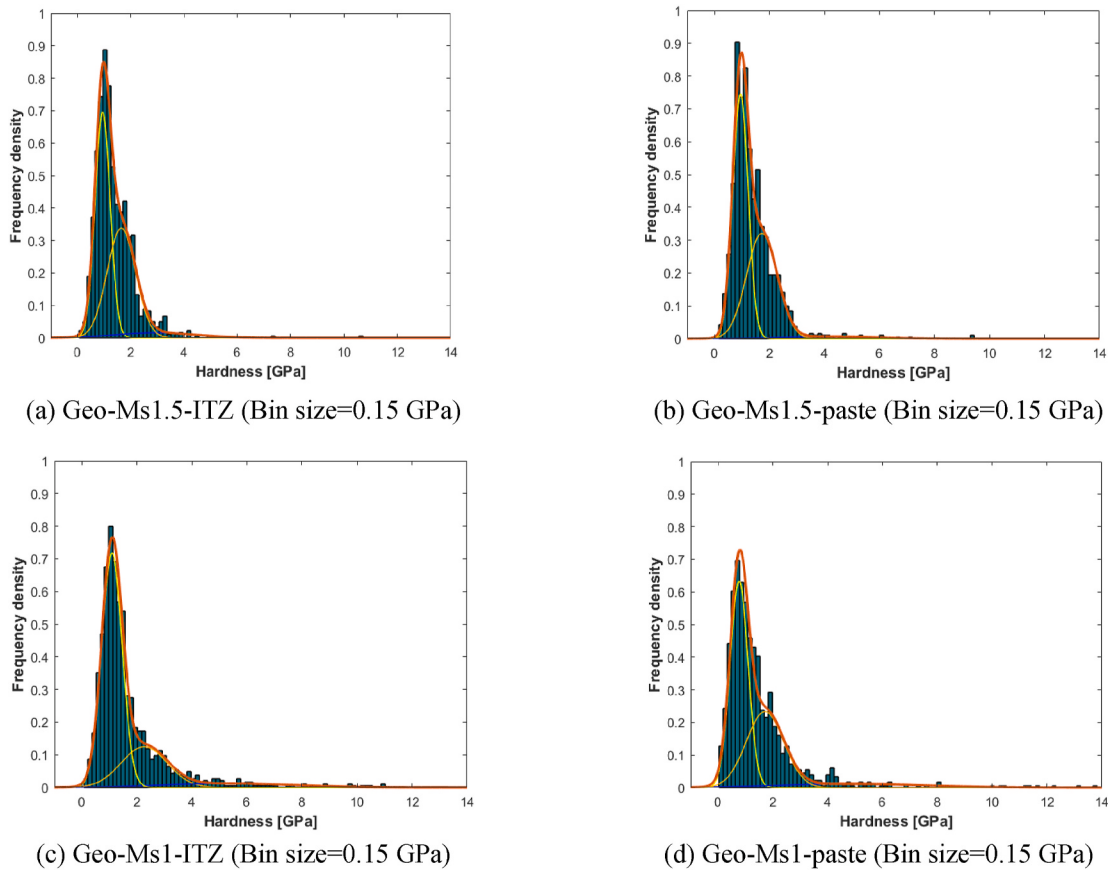


Fig. 9. Scratch hardness of ITZ and paste in geopolymers samples.

Table 4
Deconvolution results for hardness probability density distribution.

Samples	Components	Hardness (GPa)	Proportion	Standard deviation
Geo-Ms1.5-ITZ	1	0.95	49.05%	0.28
	2	1.65	45.01%	0.53
	3	2.93	5.94%	1.50
Geo-Ms1.5-paste	1	0.94	52.17%	0.28
	2	1.72	44.64%	0.56
	3	4.11	3.19%	1.89
Geo-Ms1-ITZ	1	1.10	66.48%	0.37
	2	2.27	26.09%	0.83
	3	5.34	7.43%	2.40
Geo-Ms1-paste	1	0.77	51.80%	0.33
	2	1.71	39.87%	0.68
	3	4.88	8.33%	2.81
Geo-Ms1-paste	1	0.58	30.37%	0.23
	2	1.06	32.01%	0.32
	3	1.81	25.80%	0.52
	4	3.30	9.20%	1.09
	5	7.82	2.61%	2.95

difference between ITZ and paste less significant, enabling to make better use of both parts. The benefits brought by silica modulus on ITZ coincide with previous studies using siliceous aggregates [3,4].

$$f = \pi_1 \Phi\left(\frac{m - \mu_1}{\sigma_1}\right) / \sum_{i=1}^5 \pi_i \Phi\left(\frac{m - \mu_i}{\sigma_i}\right) \quad (5)$$

where f is the proportion of data from the defect related phase shown by the purple phase in Fig. 11. The m is the hardness value of 0.407 GPa or 0.637 GPa provided in Table 5. π_i , μ_i and σ_i are the proportion, average value and standard deviation of the i th component of the five

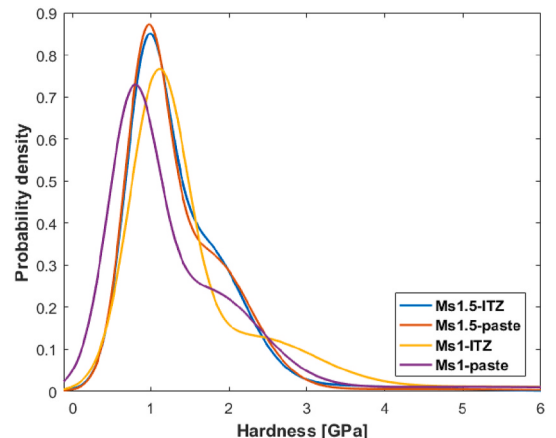


Fig. 10. The probability density distribution of scratch hardness.

components model.

3.3.4. Scratch friction coefficient of ITZ and paste

The frequency density of scratch friction coefficient distribution is shown in Fig. 12. Compared with hardness, the distribution of friction coefficient is more concentrated, which mainly varies in the range of 0–1.5. The more concentrated distribution enables a small bin size to reveal more details. The 3-component models are unable to reflect the data well. Thus, the number of components is all increased to 5, which leads to an excellent match of models with histograms. These probability distribution curves are summarized for comparison in Fig. 13.

The distribution of friction coefficient does not show strong

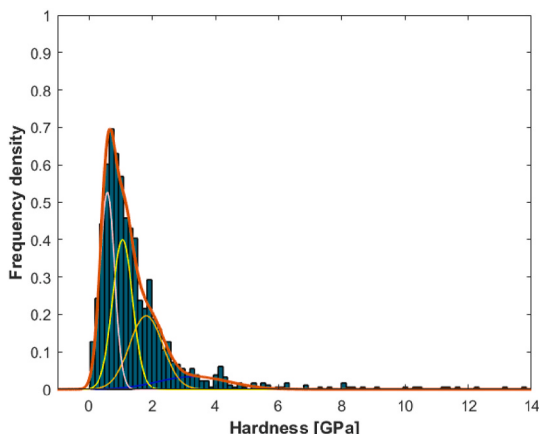


Fig. 11. Matching histograms by Gaussian mixture models with 5 components for Geo-Ms1-paste.

Table 5
Percentage of test data from large scratch widths.

Samples	$w > 5 \mu\text{m}$ ($H < 0.407 \text{ GPa}$), %	$w > 4 \mu\text{m}$ ($H < 0.637 \text{ GPa}$), %
Geo-Ms1.5-ITZ	1.66	8.65
Geo-Ms1.5-paste	1.82	7.88
Geo-Ms1-ITZ	1.94	7.46
Geo-Ms1-paste	8.45	21.21

consistency with scratch hardness. Compared with others, Ms1-paste in Fig. 10 was found to have a substantial amount of low hardness data. The same phenomenon is not observed for its friction coefficient distribution. The results listed in Table 3 indicate that only Geo-Ms1-paste displays a significantly different average scratch friction coefficient, which shows larger values than others. As analyzed previously by the 5 components model, the distinct hardness probability distribution of Ms1-paste should be caused by the defects related component, which has an average hardness of 0.58 GPa. After clustering, hardness data belonging to this component were collected. For each hardness datum, by tracking the raw test data, the corresponding friction coefficient that tested at the same scratch location can be obtained. The hardness and friction coefficient data are combined presented by scattering points in

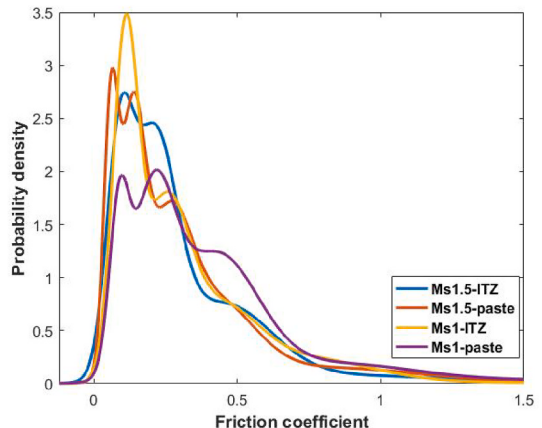
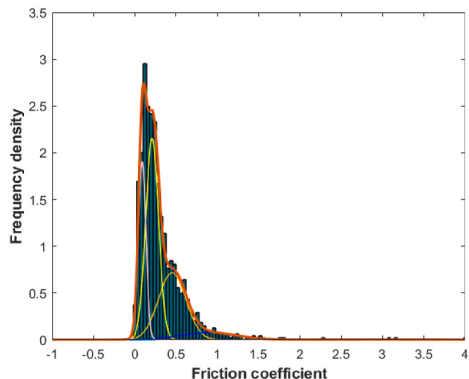
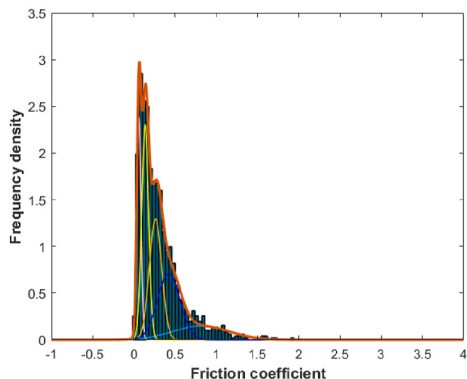


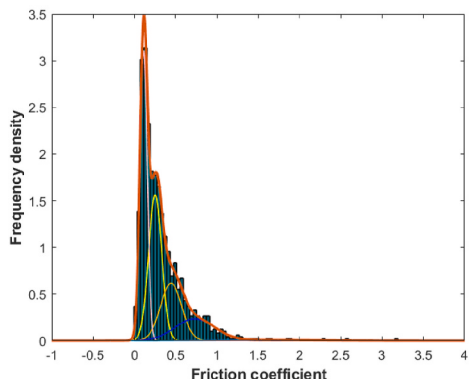
Fig. 13. The probability density distribution of scratch friction coefficient.



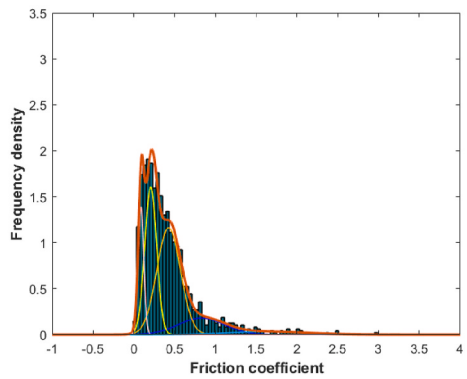
(a) Geo-Ms1.5-ITZ (Bin size=0.04 GPa)



(b) Geo-Ms1.5-paste (Bin size=0.04 GPa)



(c) Geo-Ms1-ITZ (Bin size=0.04 GPa)



(d) Geo-Ms1-paste (Bin size=0.04 GPa)

Fig. 12. Scratch friction coefficient of ITZ and paste in geopolymers samples.

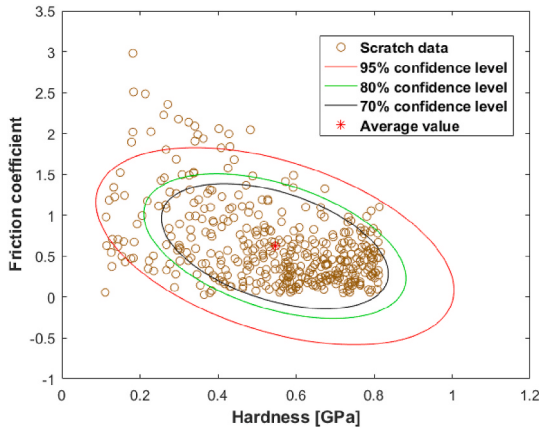


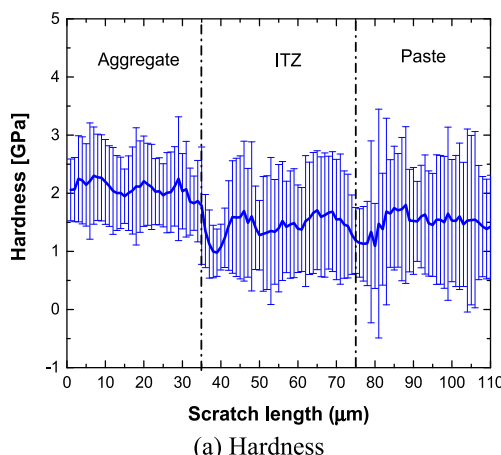
Fig. 14. Clustered hardness data and corresponding friction coefficient for the component with average hardness of 0.58 GPa.

Fig. 14. For the clustered data, the hardness is 0.55 ± 0.19 GPa, while the friction coefficient is 0.62 ± 0.49 . The hardness result indicates that although there is a slight deviation, the clustered data can still reflect the component with hardness of 0.58 GPa. The corresponding friction coefficient is found to have a very high average value and standard deviation. After removing the friction coefficient corresponding to the defects related component, the average value and standard deviation of remaining friction coefficient data are 0.31 and 0.22, respectively, which achieve similar values as other results in Table 3. Thus, the abnormally high friction coefficient of the Geo-Ms1-paste should be caused by the defects related component. A two-dimensional Gaussian distribution model [41,42] was calculated based on these data. Since just one component is used, the model provided a good evaluation on average value but deviation on variance/covariance. Nevertheless, according to the confidence ellipses, it is not questionable to know that there is a negative correlation coefficient between hardness and friction coefficient. This phenomenon is in line with scratch results on different individual micro-constituents [29], where harder constituent has a lower friction coefficient. It is attributed to different mechanisms behind the tested properties [29]: hardness is governed by composition and morphology, while fiction is affected by the topology of the contacted surface. The defects related component is destined to have a large friction coefficient. Thus, small defects in gel that have a negative impact on macro performance has been identified by scratch technique via both scratch hardness displayed in Fig. 10 and scratch friction coefficient given in Table 3.

3.3.5. Effects of scratch direction

The results of the scratch test across aggregate, ITZ and paste of geopolymer with silica modulus of 1.5 are shown in Fig. 15. The result in Fig. 15(a) shows that there is a significant difference between the hardness of aggregate and binder (ITZ and paste). The average hardness of aggregate, ITZ and paste are 2.08 ± 0.73 GPa, 1.43 ± 0.92 GPa and 1.51 ± 1.15 GPa, respectively, which all show a larger standard deviation than the results collected from test scheme I. There is also a difference between the average hardness values obtained by these two different test schemes. For this test, it was set to have a similar number of test points on each object as the scratch test parallel to ITZ (scheme I). However, the wall effect leads to properties that change gradually with increased distance to aggregate. Compared with results all collected from a constant distance to the boundary of aggregate, the average results from this kind of test would be undoubtedly more variable. The around 33 test points at each distance make the results hard to overcome the heterogeneous features. The typical evidence is the different hardness of ITZ and paste on the same locations as that in the scratch scheme I, which are obtained as 1.28 ± 0.60 GPa and 1.53 ± 1.05 GPa, respectively, in scheme II for scratch tests 15 μm and 65 μm away from aggregate. When the scratch test reaches ITZ from aggregate, the hardness value decreases rapidly and then increases. Scratch hardness in the boundary of ITZ and paste also shows low value. There are some reasons such as interfacial cracks and very low content of unreacted particles that may be able to support the low hardness of ITZ at the location near to aggregate. Different from the first boundary, the low hardness at the boundary of ITZ and paste does not indicate a successful identification of boundary by scratch test, which would be mainly attributed to the unstable results from limited test points at each given distance. After all, the term 'transition zone' means gradually changing properties. Boundary defined between 'ITZ' and 'paste' is from the location where properties tend to be stable. In addition to unstable results, another inaccuracy in scratch test II is the constraint effect, which would enhance the properties of the part of ITZ that near to aggregate. Hence, although the average value of all hardness data on each object is not significantly different from that in test scheme I, the average results from scheme II should also be more unstable.

The friction coefficient along scratch is shown in Fig. 15(b), which are 0.29 ± 0.21 , 0.48 ± 0.34 and 0.58 ± 0.42 respectively for aggregate, ITZ and paste. The average value and standard deviation obtained are all larger than that in test scheme I. For aggregate, it may be caused by a high amount of defects at the location near to boundary resulted from polish. Compared with 0.31 in scratch scheme I, the friction coefficient of ITZ and paste tested at the distance of 15 μm and 65 μm to the surface of aggregate in scratch scheme II are larger values of 0.38 ± 0.25 and 0.56 ± 0.44 , respectively. Although different directions may sometimes



(a) Hardness

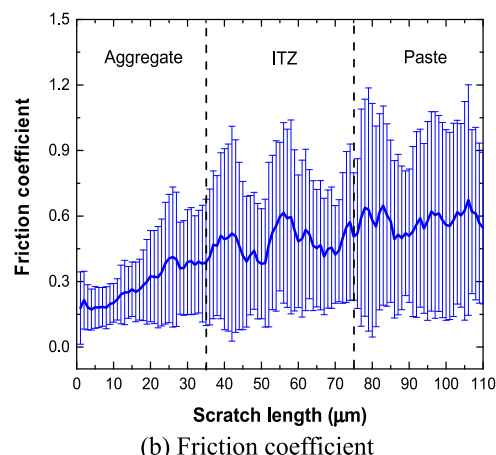


Fig. 15. Scratch test perpendicular to the boundary of modelled aggregates.

affect the friction coefficient even in the same location, the nearly one times of difference in the same paste still indicates the errors caused by the number of test data.

Thus, based on the same number of test points, scratch scheme I could provide a more reliable result for a comparison of ITZ with paste. Scratch scheme II with increased distance to aggregate has the potential to reveal the variation trend of properties but requires much more tests to eliminate the inaccuracy caused by insufficient test data on each given scratch distance. The number of test points should increase further if a smaller tip [43,44] is adopted to obtain valid data without affected by constraint effect on the part of ITZ very close to aggregate.

4. Conclusion

Based on the modelled aggregate with a neat interface, nanoscratch test was conducted on ITZ to understand mechanical properties of ITZ in geopolymer composites with different silica modulus of 1 and 1.5. The main conclusions can be drawn as below:

- (1) ITZ caused by wall effect was more distinct in geopolymer composites with silica modulus of 1. Based on the ranges in fly ash content, the size of ITZ was determined as around 30 μm and 40 μm for Geo-Ms1 and Geo-Ms1.5, respectively. The ITZ in the modelled geopolymer concrete exhibited dense microstructures and was more uniform than geopolymer paste.
- (2) Scratch hardness and scratch friction coefficient depended on the normal load applied. When slightly increased the normal load from 2 mN to 4 mN and 8 mN, the hardness was increased by 23.08% and 10.00%, respectively, while the friction coefficient was increased by 41.67% and 105.88%, respectively.
- (3) ITZ and paste of Geo-Ms1.5 showed very close scratch hardness and scratch friction coefficient. The scratch friction coefficient of ITZ and paste were 0.31 ± 0.30 and 0.31 ± 0.27 , respectively. In addition to a similar overall hardness value, the scratch hardness of the first component had a similar value of around 0.95 GPa for ITZ and paste.
- (4) For Geo-Ms1, the scratch friction coefficient was 0.32 ± 0.29 for ITZ and 0.42 ± 0.37 for paste. In the three component model, the scratch hardness of the first component was 1.10 GPa and 0.77 GPa, respectively for ITZ and paste. Compared with ITZ, the significantly lower hardness of the first component but higher overall friction coefficient of paste could be caused by defects related points.
- (5) Compared to the scratch test parallel to aggregate boundary, perpendicular scratch that continuously crosses aggregate, ITZ and paste presented the potential to reveal the detailed variation of properties with increased distance to aggregate. However, based on a similar number of test points, the properties results obtained from perpendicular scratch were less stable and reliable. Parallel scratch uniquely applicable to the modelled interface can quickly provide useful information to reflect the mechanical properties of ITZ.

CRediT authorship contribution statement

Wengui Li: Conceptualization, Investigation, Writing – review & editing, Resources, Supervision. **Zhiyu Luo:** Investigation, Writing – original draft. **Yixiang Gan:** Writing – review & editing. **Kejin Wang:** Writing – review & editing. **Surendra P. Shah:** Writing – review & editing.

Declaration of competing interest

The authors declare that they have no known competing financial interests or personal relationships that could have appeared to influence the work reported in this paper.

Acknowledgement

The authors appreciate the Australian Research Council, Australia (DE150101751; IH200100010; LE210100019), and University of Technology Sydney Research Academic Program at Tech Lab (UTS RAPT).

References

- [1] J.L. Provis, J.S. Van Deventer, Alkali Activated Materials: State-Of-The-Art Report, RILEM TC 224-AAM, Springer Science & Business Media, 2013.
- [2] Z. Zhang, J.L. Provis, A. Reid, H. Wang, Fly ash-based geopolymers: the relationship between composition, pore structure and efflorescence, *Cement Concr. Res.* 64 (2014) 30–41.
- [3] W. Lee, J. Van Deventer, The interface between natural siliceous aggregates and geopolymers, *Cement Concr. Res.* 34 (2) (2004) 195–206.
- [4] W. Lee, J. Van Deventer, Chemical interactions between siliceous aggregates and low-Ca alkali-activated cements, *Cement Concr. Res.* 37 (6) (2007) 844–855.
- [5] M. Khedmati, Y.-R. Kim, J.A. Turner, H. Alanazi, C. Nguyen, An integrated microstructural-nanomechanical-chemical approach to examine material-specific characteristics of cementitious interphase regions, *Mater. Char.* 138 (2018) 154–164.
- [6] M. Khedmati, Y.-R. Kim, J.A. Turner, Investigation of the interphase between recycled aggregates and cementitious binding materials using integrated microstructural-nanomechanical-chemical characterization, *Compos. B Eng.* 158 (2019) 218–229.
- [7] Z. Luo, W. Li, K. Wang, A. Castel, S.P. Shah, Comparison on the properties of ITZs in fly ash-based geopolymer and Portland cement concretes with equivalent flowability, *Cement Concr. Res.* 143 (2021), 106392.
- [8] Z. Luo, W. Li, K. Wang, S.P. Shah, Research progress in advanced nanomechanical characterization of cement-based materials, *Cement Concr. Compos.* 94 (2018) 277–295.
- [9] C. Hu, Z. Li, A review on the mechanical properties of cement-based materials measured by nanoindentation, *Construct. Build. Mater.* 90 (2015) 80–90.
- [10] W. Li, J. Xiao, Z. Sun, S. Kawashima, S.P. Shah, Interfacial transition zones in recycled aggregate concrete with different mixing approaches, *Construct. Build. Mater.* 35 (2012) 1045–1055.
- [11] J. Xiao, W. Li, Z. Sun, D.A. Lange, S.P. Shah, Properties of interfacial transition zones in recycled aggregate concrete tested by nanoindentation, *Cement Concr. Compos.* 37 (2013) 276–292.
- [12] P.G. Allison, C. Weiss Jr., R.D. Moser, A. Diaz, O.G. Rivera, S.S. Holton, Nanoindentation and SEM/EDX characterization of the geopolymer-to-steel interfacial transition zone for a reactive porcelain enamel coating, *Compos. B Eng.* 78 (2015) 131–137.
- [13] R.F. Gibson, A review of recent research on nanoindentation of polymer composites and their constituents, *Compos. Sci. Technol.* 105 (2014) 51–65.
- [14] A. Urena, J. Rams, M. Escalera, M. Sanchez, Characterization of interfacial mechanical properties in carbon fiber/aluminium matrix composites by the nanoindentation technique, *Compos. Sci. Technol.* 65 (13) (2005) 2025–2038.
- [15] Q. Li, Y. Li, L. Zhou, Nanoscale evaluation of multi-layer interfacial mechanical properties of sisal fiber reinforced composites by nanoindentation technique, *Compos. Sci. Technol.* 152 (2017) 211–221.
- [16] Z. Liu, C. Cai, H. Peng, F. Fan, Experimental study of the geopolymeric recycled aggregate concrete, *J. Mater. Civ. Eng.* 28 (9) (2016), 04016077.
- [17] T. Ji, Q. Gao, W. Zheng, X. Lin, H.-C. Wu, Interfacial transition zone of alkali-activated slag concrete, *ACI Mater. J.* 114 (3) (2017).
- [18] B. Beake, A. Harris, T. Liskiewicz, Review of recent progress in nanoscratch testing, *Tribology-Materials, Surf. Interfaces* 7 (2) (2013) 87–96.
- [19] J. Liu, Q. Zeng, S. Xu, The state-of-art in characterizing the micro/nano-structure and mechanical properties of cement-based materials via scratch test, *Construct. Build. Mater.* 254 (2020), 119255.
- [20] X. Wang, P. Xu, R. Han, J. Ren, L. Li, N. Han, F. Xing, J. Zhu, A review on the mechanical properties for thin film and block structure characterised by using nanoscratch test, *Nanotechnol. Rev.* 8 (1) (2019) 628–644.
- [21] M. Schöneich, M. Zamanzade, M. Stommel, Fiber-matrix interphase in applied short glass fiber composites determined by a nano-scratch method, *Compos. Sci. Technol.* 119 (2015) 100–107.
- [22] A. Dasari, Z.-Z. Yu, Y.-W. Mai, Fundamental aspects and recent progress on wear/scratch damage in polymer nanocomposites, *Mater. Sci. Eng. R Rep.* 63 (2) (2009) 31–80.
- [23] G. Mallikarjunachari, P. Ghosh, Analysis of strength and response of polymer nano thin film interfaces applying nanoindentation and nanoscratch techniques, *Polymer* 90 (2016) 53–66.
- [24] J.A. King, I. Miskioglu, D.D. Wright-Charlesworth, C.D. Van Karsen, Nanoscratch testing to assess the fiber adhesion of short-carbon-fiber composites, *J. Appl. Polym. Sci.* 103 (1) (2007) 328–335.
- [25] S. Zhao, E. Van Dam, D. Lange, W. Sun, Abrasion resistance and nanoscratch behavior of an ultra-high performance concrete, *J. Mater. Civ. Eng.* 29 (2) (2017), 04016212.
- [26] S. Du, Y. Jiang, J. Zhong, Y. Ge, X. Shi, Surface abrasion resistance of high-volume fly ash concrete modified by graphene oxide: macro-and micro-perspectives, *Construct. Build. Mater.* 237 (2020), 117686.

- [27] J. Xu, W. Yao, Nano-scratch as a new tool for assessing the nano-tribological behavior of cement composite, *Mater. Struct.* 44 (9) (2011) 1703–1711.
- [28] Z.-z. Wang, P. Gu, X.-p. Wu, H. Zhang, Z. Zhang, M.Y. Chiang, Micro/nano-wear studies on epoxy/silica nanocomposites, *Compos. Sci. Technol.* 79 (2013) 49–57.
- [29] A.-T. Akono, J. Chen, S. Kaewunruen, Friction and fracture characteristics of engineered crumb-rubber concrete at microscopic lengthscale, *Construct. Build. Mater.* 175 (2018) 735–745.
- [30] A.-T. Akono, N.X. Randall, F.-J. Ulm, Experimental determination of the fracture toughness via microscratch tests: application to polymers, ceramics, and metals, *J. Mater. Res.* 27 (2) (2012) 485–493.
- [31] C.G. Hoover, F.-J. Ulm, Experimental chemo-mechanics of early-age fracture properties of cement paste, *Cement Concr. Res.* 75 (2015) 42–52.
- [32] J. Liu, Q. Zeng, S. Xu, Is scratch test proper to characterize microstructure and mechanical properties of cement-based materials? The effects of loading level and routine, *Cement Concr. Res.* 133 (2020), 106072.
- [33] A. Karimzadeh, M. Ayatollahi, Investigation of mechanical and tribological properties of bone cement by nano-indentation and nano-scratch experiments, *Polym. Test.* 31 (6) (2012) 828–833.
- [34] Y. Mao, W. Yao, J. Xu, Study on the Unhydrated Cement Grain/CSH Gel Interface in Cement Paste by Use of Nano-Scratch Technique, Key Engineering Materials, Trans Tech Publ, 2013, pp. 84–88.
- [35] J. Xu, D.J. Corr, S.P. Shah, Nanoscratch study of the modification effects of NanoSiO₂ on C–S–H gel/cement grain interfaces, *J. Mater. Civ. Eng.* 29 (9) (2017), 04017093.
- [36] K.L. Scrivener, A.K. Crumbley, P. Laugesen, The interfacial transition zone (ITZ) between cement paste and aggregate in concrete, *Interface Sci.* 12 (4) (2004) 411–421.
- [37] K.L. Scrivener, Backscattered electron imaging of cementitious microstructures: understanding and quantification, *Cement Concr. Compos.* 26 (8) (2004) 935–945.
- [38] S. Diamond, Considerations in image analysis as applied to investigations of the ITZ in concrete, *Cement Concr. Compos.* 23 (2–3) (2001) 171–178.
- [39] K. Wu, H. Shi, L. Xu, G. Ye, G. De Schutter, Microstructural characterization of ITZ in blended cement concretes and its relation to transport properties, *Cement Concr. Res.* 79 (2016) 243–256.
- [40] J.J. Chen, L. Sorelli, M. Vandamme, F.J. Ulm, G. Chanvillard, A Coupled nanoindentation/SEM-EDS study on low water/cement ratio Portland cement paste: evidence for C-S-H/Ca(OH)₂ nanocomposites, *J. Am. Ceram. Soc.* 93 (5) (2010) 1484–1493.
- [41] Z. Luo, W. Li, Y. Gan, K. Mendu, S.P. Shah, Maximum likelihood estimation for nanoindentation on sodium aluminosilicate hydrate gel of geopolymers under different silica modulus and curing conditions, *Compos. B Eng.* 198 (2020), 108185.
- [42] Z. Luo, W. Li, Y. Gan, K. Mendu, S.P. Shah, Applying grid nanoindentation and maximum likelihood estimation for NASH gel in geopolymers paste: Investigation and discussion, *Cement Concr. Res.* 135 (2020), 106112.
- [43] Y. Yan, S. Chang, T. Wang, Y. Geng, Scratch on polymer materials using AFM tip-based approach: a review, *Polymers* 11 (10) (2019) 1590.
- [44] M. Zhou, Y. Jiang, Y. Sui, Microstructure and properties of interfacial transition zone in ZTA particle-reinforced iron composites, *Appl. Phys. A* 125 (2) (2019) 110.